DOI: 10.1002/ejic.200900134

Preparation of TiN_xO_{2-x} Photoelectrodes with NH_3 Under Controllable Middle Pressures for Dye-Sensitized Solar Cells

Xin Wang,[a] Yulin Yang,*[a] Zhaohua Jiang,[a] and Ruiqing Fan[a]

Keywords: Doping / Nanotechnology / Solar cells / Structure-activity relationships / Titanium / Metal oxynitride

As part of our efforts to find a way to control the concentration of N-doped TiO_2, TiN_xO_{2-x} powders were prepared by a device of our own design. In this research, photoelectrodes are generated using N-doped TiO_2 materials where the concentrations are adjusted by the amount of NH_3 under middle pressure, which is seldom reported. Considerable efforts have been directed to the study of the optical absorption edge that is redshifted towards the visible-light region. Therefore, N-doped TiO_2 electrodes are characterized by SPS and TPV analyses as experimental and theoretical studies. Experimental results indicate that the band gap of the semiconductor has been narrowed by increasing the concentration of the N-doped TiO_2. The overall conversion efficiency of the solar cell has shown that the photoelectrical properties of the N-doped TiO_2 have greatly improved with different concentrations. It can therefore be concluded that the synthesis route we found through this study is an effective way to adjust the relationship between the concentration and the band gap of the N-doped TiO_2 photoelectrodes.

Introduction

Metal oxynitrides can be described as derivatives of the oxides, formed by the simultaneous substitution of the cationic and anionic components. For example, since O'Regan and Grätzel developed solar cells based on the nanocrystalline TiO_2 electrode,[1] dye-sensitized solar cells (DSCs) have attracted much attention for their relatively low cost and high photoelectrical properties.[2–5] A variety of methods have been devised to fabricate nanoscale TiO_2 film electrodes to obtain high energy conversion efficiency for solar cells, such as replacing with liquid electrolytes,[6] doping atoms in TiO_2,[7] improving the performance of the dye,[8] etc. Considerable efforts have been directed to the synthesis of doped TiO_2 with the optical absorption edge red-shifted towards the visible-light region. Nitrogen-doped TiO_2 has been investigated by experimental and theoretical approaches[9–13] since it was proposed by Asahi et al.[14] In recent years, a variety of methods have been reported on the visible-light photocatalysis of N-doped TiO_2, such as the sputtering of a TiO_2 target in a N_2/Ar gas mixture,[15] oxidation of TiN,[16] hydrolysis of TiO_2 tetrachloride with a nitrogen containing base,[17] amination of TiO_2 particles,[18] nitrogen ion implantation,[19] chemical vapor deposition,[20] sol–gel,[21] and decomposition of N-containing metal-organic precursors,[22] etc. Among the abundant reasonable designs, Ma et al. reported that a N-doped TiO_2 electrode could be used to improve the overall conversion efficiency (η) in 2005.[23] However, these methods showed that there was no effective way to adjust the relationship between the concentration and the band gap of the N-doped TiO_2. As part of our efforts to find a way to control the composition of N-doped TiO_2, we designed a device to generate TiN_xO_{2-x} powders using NH_3 as a gaseous precursor. The photoelectrical properties of N-doped TiO_2 electrodes are characterized by XPS, XRD, Raman spectroscopy, SEM, TPV, and SPS analysis under different reaction temperatures and middle pressures for different time lengths. However, when the interfacial electrons are located in the nanoscale environments their transferring behavior associated with the spatial heterogeneities become complex. Herein, the research has also offered a photoelectrochemical analysis to prove the relationships amongst the concentration, the band gap, the nanoparticles size and the photoelectric conversion efficiency of the N-doped TiO_2 photoelectrodes.

Results and Discussion

Characterization of the Phase Structure

As shown in the Supporting Information, the XRD patterns of TiN_xO_{2-x} indicate that the pressure and time are not evidence effective to the change of phase composition as compared with the temperature. The crystal structure of nitrogen-doped TiO_2 is in general similar to that of TiO_2, as shown in Figure 1. The strong absorption diffraction

[a] Department of Chemistry, Harbin Institute of Technology, Harbin 150001, P. R. China
Fax: +86-451 86418270
E-mail: ylyang@hit.edu.cn

Supporting information for this article is available on the WWW under http://dx.doi.org/10.1002/ejic.200900134.

peaks are assigned to the anatase type over a temperature range of 400–500 °C, while the rutile phase is observed only at temperatures above 600 °C. These results are in good agreement with the results obtained from Raman spectroscopy.

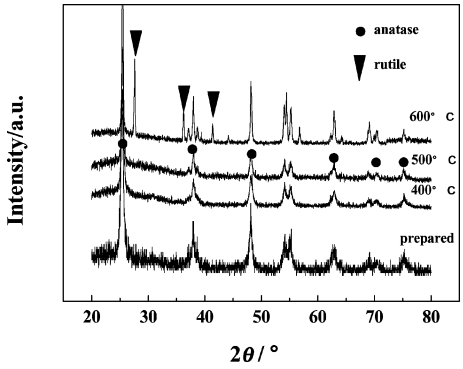

Figure 1. XRD patterns of raw TiO_2 and N-doped powders at different temperatures.

Figure 2 shows five active fundamental modes around 151 (E_g), 204 (E_g), 399 (B_{1g}), 515 (A_{1g}, B_{1g}), and 639 cm^{-1} (E_g), which belong to the anatase phase. Further sintering at higher temperatures causes the transformation of the anatase phase to the rutile phase, confirmed by the appearance of the peaks at 453 (E_g) cm^{-1}. As shown in Table 1, the anatase-phase sample has more active photoelectric properties than the rutile phase, which is in good agreement with the result reported by Park et al.[24] For dye-sensitized solar cells the anatase phase of TiO_2 is the desired crystalline phase because it has more appropriate optical and electronic properties compared with the rutile phase.

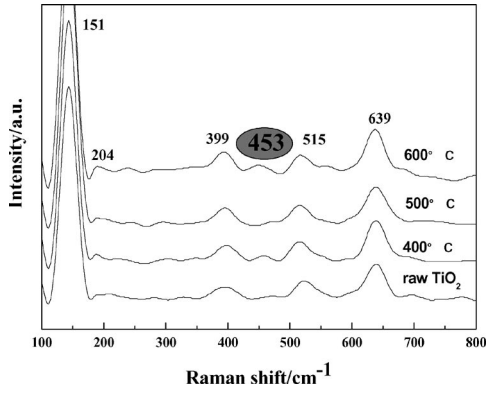

Figure 2. Raman spectra of raw TiO_2 and N-doped TiO_2 powders at different temperatures.

Composition Analysis

However, the nanostructure is not the only determinant for the differences between TiN_xO_{2-x} photoelectrodes. Whether the concentration of nitrogen-doped photoelectrodes plays an important role in DSCs is discussed from the XPS results. Table 1 demonstrates that a slightly high efficiency emerged by increasing the concentration of the nitrogen doped in the samples. Moreover, it also represents the general relationships involving the η values of the TiO_2-based DSCs, the concentration of the N-doped TiO_2, the band gap, the crystalline size of the samples, and the reaction conditions in the TiO_2 film electrodes.

As shown in Figure 3, the results represent two differential peaks of N that are centered at 396 eV and 400 eV. The 400 eV band is attributed to molecularly chemisorbed dinitrogen γ-N_2. The 396 eV peak is assigned as atomic β-N bonded to Ti, that is, when N substitutionally replaces O then sites are associated with atomic N.

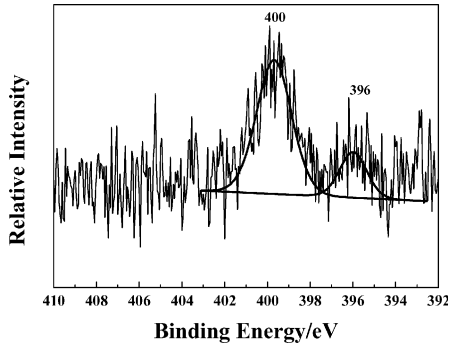

Figure 3. The XPS spectra of the N 1s core level of the N-doped TiO_2 powders treated at 400 °C for 24 h at 0.8 MPa.

It is reported that a few requirements are needed to achieve visible-light activity for N-doped TiO_2:[25] (i) doping should produce states in the band gap of TiO_2 that absorb visible light; (ii) the dopant states of doped TiO_2 should form a narrow N 2p band above the valence band (VB) of TiO_2 to ensure photoreductive activity.

Table 1. Contrast of DSC performances and the structure of TiN_xO_{2-x} photoelectrodes.

		T [°C] (24 h, 0.8 MPa)			*t* [h] (500 °C, 0.4 MPa)		*p* [Mpa] (600 °C, 12 h)	
	Undoped TiO_2	400	500	600	12	24	0.4	0.6
V_{oc} [mV]	535	574	597	568	527	540	582	510
J_{sc} [mA cm^{-2}]	1.32	6.88	5.49	4.72	5.63	5.34	2.86	1.44
FF	0.58	0.63	0.58	0.62	0.51	0.56	0.58	0.41
η [%]	2.12	6.20	4.75	4.18	3.76	4.05	2.41	0.76
N-Doped concentration [%]	–	1.22	0.87	0.66	0.60	0.70	0.52	0.46
Band gap [eV]	3.20	2.62	2.63	2.86	2.88	2.80	2.91	3.08
Crystal size [nm]	25–50	18	20	25	29	24	32	36

Table 1 indicates that the concentration of N-doped TiO_2 has been increased with a longer sintering time or lower temperature or less pressure. The results also show that high concentrations of N-doped TiO_2 could lead to higher visible-light activity. It is difficult for the N atom to be inserted into the TiO_2 crystal lattice because of it metamorphosing under the pressure of a gas–solid reaction. With an increase in the temperature the movement of the gas molecules was excited, which was of no benefit to the N atoms in the TiO_2 lattice and the concentration of N-doped TiO_2 decreased. However, a longer sintering time was favorable for the stabilization of the N-doped atoms. In other words, the concentration of N-doped TiO_2 decreased with the enhancement of pressure, while it increased with longer sintering time or lower temperature.

Considering the effect of the three factors of the gas–solid reaction, the reaction was hypothesized to be as follows:

$$NH_3 + TiO_2 \rightarrow TiN_xO_{2-x} + H_2O \quad (1)$$

During the N replacement of O in the TiO_2 lattice, NH_3 played a role as a kind of reducer, where it was involved in adjusting the quantity balance of the oxygen vacancies and dopant N. Because of the increase of x in TiN_xO_{2-x}, the oxygen vacancies act as recombination centers for e^- and h^+, which led to lower visible-light activity. In this case, a suitable ratio between the oxygen vacancies and dopant N determined the photoelectrical properties of the N-doped TiO_2 material.

The Surface Photovoltage Spectrum Analysis

On irradiating with visible light, the quantum yields increased with the concentration of nitrogen, suggesting that the intragap states should sufficiently overlap with the band states of TiO_2. This result caused photoexcited carriers (e^-) to be transferred to reactive sites at the TiO_2 surface within their lifetime.

The surface photovoltage spectrum (SPS) method is commonly applied to TiO_2 for dye-sensitized solar cells, which is a well-established noncontact technique for surface-state distribution.[26–28] As shown in Figure 4, the SPS analysis for samples with the N719 dye demonstrates that one typical characteristic response band close to 350 nm, which originates from the band–band electron transition of TiO_2, is observed. The absorption band in the visible-light region originates from the N719 dye absorbed in TiO_2. However, for N-doped TiO_2 samples, a new SPS signal from 400 to 550 nm is observed, which can be assigned to the band–band electron transition of the N-doped band (the UV/Vis spectra are shown in the Supporting Information). The results show that the N-doped TiO_2 with a lower concentration has a similar UV/Vis spectrum to that of TiO_2, and only redshifts after the reaction in NH_3. However, a new peak around 470 nm appears with a higher N concentration, which provides proof that N is doped in the lattices and affects its visible-light activity. The presence of the new signal is probably caused by the N-doped band, where the visible-light response range is broadened and continuous after being sensitized by the dye. The band gap is calculated from the formula: E_{gap} (eV) = 1240/λ_{max} (nm), where E_{gap} is the band gap and λ_{max} represents the edge of the maximal response absorption band. This phenomenon provides clear evidence that a higher concentration of N-doped TiO_2 could result in a narrower band gap.[29] Moreover, the solar cell that has been produced with a narrower band gap shows considerable improvement in the short-circuit current and efficiency as a function of the N-doped TiO_2 lattice.

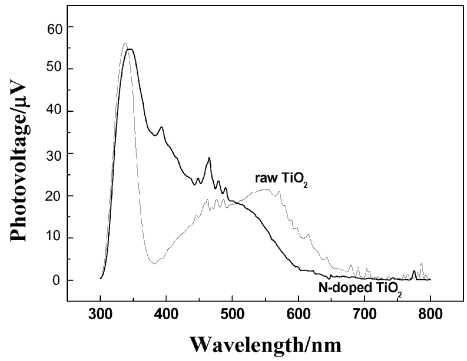

Figure 4. SPS spectrum of raw TiO_2 and N-doped samples with the N719 dye.

In addition, it is also observed that the surface morphology is related to the amount of N doped in the TiO_2. The grain sizes in such samples gradually increase from 10 to 50 nm, according to SEM micrographs, after sintering over a temperature range of 400–600 °C for 12 or 24 h. Figure 5 illustrates that the average size of the nanocrystal has

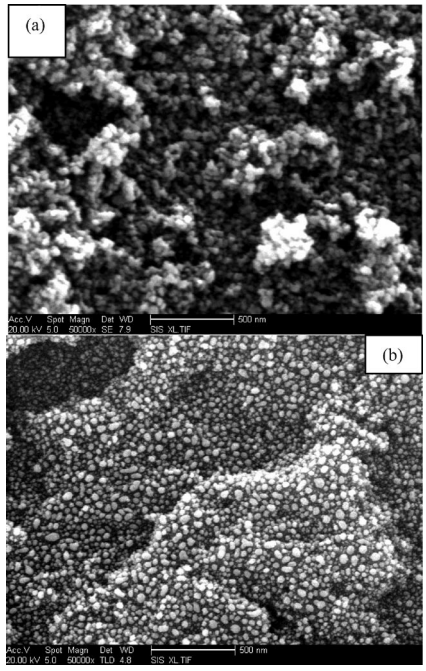

Figure 5. SEM micrographs of (a) raw TiO_2; (b) N-doped TiO_2 powders digested at 400 °C for 24 h under 0.8 MPa. The N-doped particles are approximately 20 nm and are sphere-like.

become smaller and more equal after thermal treatment. A further increase of the concentration of the N doping decreases the size of the grains (as shown in Table 1). Therefore, higher N-doped concentrations in the precursor reaction result in a decrease of the grain size. Also, the approximate nanoparticle diameter changes under different reaction conditions. On the basis of earlier studies[30] these results can be explained by the theory that the rate of crystal growth is relevant to the outside environment, such as pressure and time.

Photoelectrochemical Measurements

Figure 6 shows the performance of the DSCs in terms of J_{sc} and V_{oc} at different temperatures, pressures, and sintering time lengths, respectively. The results in Table S1 indicate that the η values of the DSCs increase with longer sintering times. However, the electrode prepared under higher pressure does not have any advantage over the one prepared under lower pressure. For example, when comparing the two samples prepared under 0.4 MPa and 0.6 MPa the latter one gives a slightly lower η value for the solar cell. The results also reveal that the η values of N-doped samples are significantly enhanced at low temperatures. It is believed that low temperatures favor the replacement of O for atomic N in TiO_2. In other words, the η values of the DSCs are enhanced with an increase in the concentration of the N-doped TiO_2.

The Transient Photovoltage Analysis

The transient photovoltage (TPV) technique is a useful method for the investigation of the dynamic behavior of photo-induced charge carriers (PICCs) in semiconductor materials, which dominates the performance of the DSCs. We can directly obtain information about the charge dynamics, including generation, separation, and recombination of photo-induced charges, by the TPV technique.

The photovoltage (PV) arises whenever light-induced excess charge carriers are separated in space. The excitation of excess carriers of charge is performed with photons of $hv > E_g$. The sign of the PV transients is positive. The positive sign implies that the photoexcited electrons move faster than holes towards the N-doped TiO_2/SnO_2:F interface. No PV signal could be detected for $hv < E_g$.

It is also considered to be an important effect of the recombination between injected carriers and holes in the charge transport. Figure 7 displays retardation due to the effect of recombination in TiO_2. The retardation of the transient PV in N-doped TiO_2 differs drastically from the material that is not N doped. The PV transients do not decay purely by exponential or logarithmic laws. A lifetime of charge carriers could be introduced for exponential decay while the recombination of specially separated charge could be used to describe a logarithmic decay.[31] The feature originated from the back diffusion of electrons inserted in the TiO_2 lattice. At the initial time, the large gradient induced by the injected electrons could finish the diffusion toward the back contact. This reverse gradient also produces back

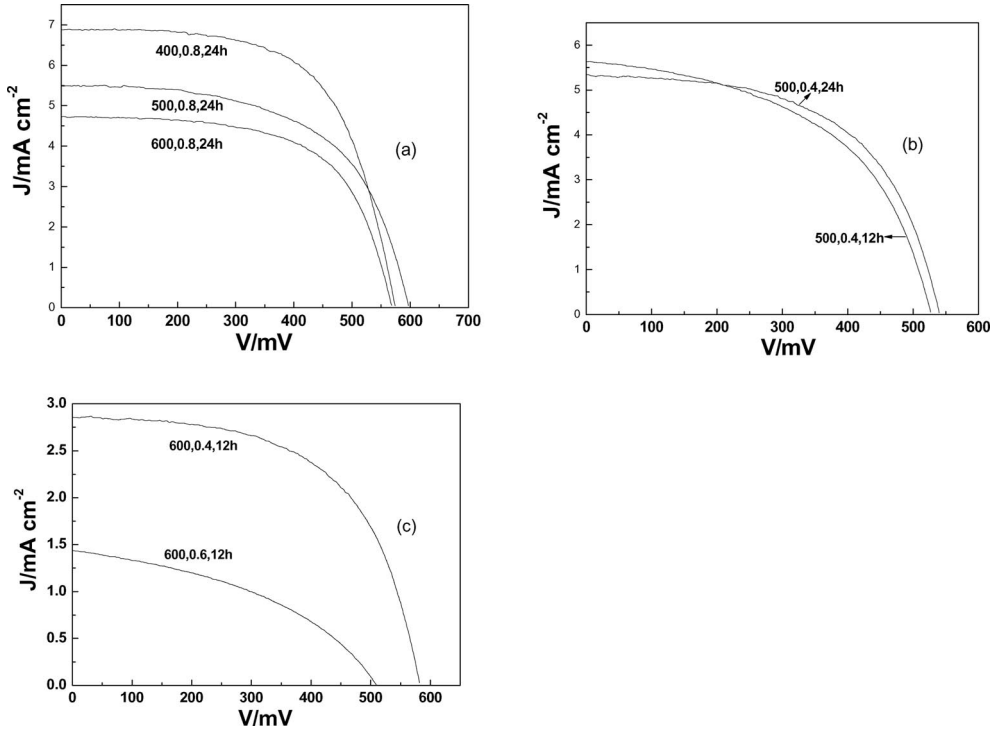

Figure 6. *J–V* (current density–voltage) curves for the sunlight-illuminated dye-sensitized solar cells under different reaction conditions. (a) Different temperatures: 400, 500 and 600 °C; (b) different times:12 h and 24 h; (c) different pressures: 0.4 MPa and 0.6 MPa.

diffusion of the electrons to the region with high recombination probability, leading to the fast decay observed in Figure 7. The gradient of excess electron and hole concentrations is caused by the non-homogeneous nature of the N-doped TiO_2 sample.

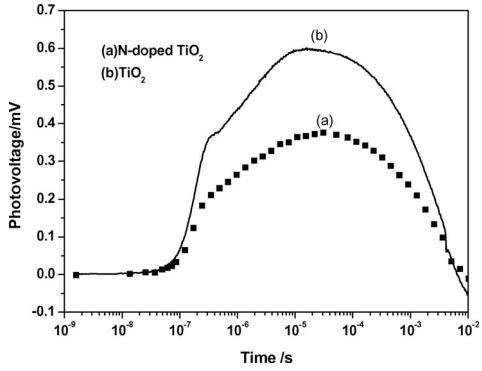

Figure 7. The photovoltage transients of the electrodes: (a) N-doped TiO_2 sample, (b) TiO_2 sample without N atoms; the wavelength and the intensity of the laser are 355 nm and 50 μJ, respectively.

The narrowing of the forbidden-gap leads to an increase of the amplitude of the spectral PV and to a much stronger retardation of the PV transients. The retardation behavior of the PV transients changes dramatically after the generation of N-dopant band states. Since the optical band gap (E_g) of TiO_2 is 3.2 eV, excitation under 355 nm (photon energy $h\nu$ = 3.5 eV) leads to a band-to-band transition. We can use a diagram to describe the energy band at the interface, which originates from the presence of intragap-dopant states above the upper level of the VB band in TiO_2 (Figure 8). This indicates that the electrons are transferred away from the injection region and diffuse to the high recombination region in the forbidden-gap, producing the fast decay observed at longer times. That is to say, the intragap-dopant states benefit the separation of e^- and h^+ and the increase of quantum yields in N-doped TiO_2.

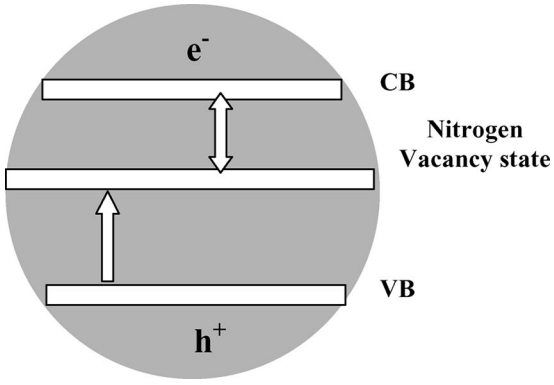

Figure 8. A diagram of band states at the interface in N-doped TiO_2.

Combining all the experimental results above, it can safely be concluded that the band gap narrowing has a greater effect on the performance of the solar cells than the effect of the recombination between injected carriers and holes in the N-doped TiO_2 material.

Conclusions

As part of our efforts to find a way to control the concentration of N-doped TiO_2, TiN_xO_{2-x} powders were prepared by a device of our own design. Photoelectrodes were generated using the N-doped TiO_2 material and the concentrations were adjusted by the amount of NH_3 used under middle pressure. Experimental results provide clear evidence that higher concentrations of N-doped TiO_2 result in a narrower band gap, since the redshifted absorption edges originate from the presence of intragap-dopant states above the upper level of the VB band. Therefore, the photoelectrode with a narrower band gap shows considerable improvement in the short-circuit current and the overall conversion efficiency as a function of the N-doped TiO_2. To sum up, it can be concluded that the research has offered proof of the relationships among the concentration, the band gap, the nanoparticle size, and the photoelectric conversion efficiency of the N-doped TiO_2 photoelectrodes. The grain sizes in the N-doped TiO_2 film are controlled by the concentration of N-doped TiO_2, which are in the range of 10–50 nm. The photoelectrochemical property of solar cells appears to be highly sensitive to the concentration of N doped in the TiO_2. The nanoparticle size, excellent anatase phase, and suitable concentrations of nitrogen doped TiO_2 are all controlled by different middle pressures, temperatures, and sintering time lengths. And so, they all affect the overall conversion efficiency of the solar cells. It is hoped that this will offer an effective way to adjust the relationship between the concentration and the band gap of the N-doped TiO_2 photoelectrodes and find underlying applications of solar cells and other photocatalytical fields.

Experimental Section

Materials: Titanium isopropoxide, LiI, 4-*tert*-butylpyridine, acetonitrile, and propylene carbonate were purchased from Aldrich Chemical Company and the dye N719 was used as received from Solaronix Company.

Preparation: Nanocrystalline titania powders were synthesized by a hydrothermal method with titanium isopropoxide used as the titanium source. The powder was then treated at different temperatures under NH_3 gas at different pressures in a sealed steel autoclave designed by ourselves.

After being cooled to room temperature, polyethylene glycol [PEG, molecular weight (MW) of 600, made in China] was added to a slurry in ethanol at a proportion of 10% TiN_xO_{2-x} powders. After that, films on FTO glasses were prepared by a screen-printed method and gradually sintered at 450 °C under dry air for device fabrication.

This research has focused on finding a set of reaction conditions that could be used to yield photochemically active products. In the sealed environment of a middle-pressure NH_3 reaction, the output performance of the solar cell is affected by the nanostructure and photoelectric properties of the N-doped TiO_2 material. Hence, the

investigation focuses on the process of the thermal doping treatment. As shown in Figure 9, the samples were prepared in a sealed stainless steel chamber (part 1). The NH_3 gas (99%, part 3) flowed into the chamber through a device (part 2) that absorbed impurities in the NH_3. The heater power was not launched until the pressure reached the predetermined values. When the temperature reached the range 400–600 °C conditions were maintained for 12 or 24 h depending on the experiment. Conditions for the thermal treatment of powders were investigated by changing the reaction temperature, time, and pressure. In order to simplify and reduce the number of variables, three sets of remarkable sintering routes on the film composition were proposed as follows: 400/500/600 °C, 0.8 MPa, 24 h; 500 °C, 0.4 MPa, 12/24 h; 600 °C, 0.4/0.8 MPa, 12 h.

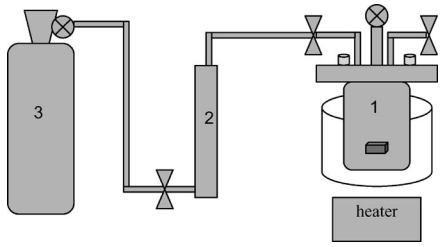

Figure 9. Self-designed device for the surface treatment of N-doped TiO_2 powders. Part 1: Sealed stainless steel chamber. Part 2: A device absorbing impurities from the NH_3. Part 3: The compressed gas cylinder of NH_3 (99%).

Characterization: The phase structure of the plasma-treated powders was characterized by X-ray diffraction (JDX-3530M, Japan) using Ni-filtered Cu-K_α radiation. The X-ray photoelectron spectroscopic results were obtained from a Thermo ESCALAB-250 spectrometer with an Al-K_α source, equipped with an ultra-high vacuum (UHV) at 3.5×10^{-7} Pa. The surface morphology of the raw and the processed powders was observed using a scanning electron microscope (SEM S-IRION, American-FEI Company; Hitachi S-4800). The Powder Raman spectra were collected with an RFS 100FT-Raman spectrometer, Bruker Company, with an optical laser at an excited wavelength of 1064 nm and exported electric power at 20 mW. The SPS instrument was assembled at Jilin University, monochromatic light was obtained by passing light from a 500-W xenon lamp (CHF-XQ500W, made in China) through a double-prism monochromator (SBP300, China). The transient photovoltage (TPV) tests were excited with a laser radiation pulse (wavelength of 355 nm and pulse width of 5 ns) from a third-harmonic Nd:YAG laser (Polaris II, New Wave Research, Inc.). The slit widths of entrance and exit were 2 and 1 mm, respectively. A lock-in amplifier (SR830, USA), synchronized with a light chopper (SR540, USA), was employed to amplify the photovoltage signal.

Photoelectrochemical Measurements: The sample was sandwiched between two FTO glass electrodes. Optically transparent electrodes were made from an F-doped SnO_2-coated glass plate (FTO, 90% transmittance in the visible, 15 Ω^{-1} per cm^2) purchased from Geao Equipment Company, Wu Han. The electrolyte used in this work was 0.5 M LiI + 0.05 M I_2 + 0.1 M 4-*tert*-butylpyridine in 1:1 (volume ratio) acetonitrile/propylene carbonate. The films were stained by immersing them into a 3×10^{-4} M solution of N719 in absolute ethanol for about 12 h. The photovoltaic performance was measured by using a mask with an aperture area of 0.12 cm^2 and the irradiance of sunlight was 40 mW cm^{-2}.

Based on the *J–V* curve, the fill factor (*FF*) is defined as $FF = (J_{max} \times V_{max})/(J_{sc} \times V_{oc})$, where J_{max} and V_{max} are the photocurrent density and photovoltage for maximum power output, respectively, (J_{sc} and V_{oc} are the short-circuit photocurrent density and open-circuit photovoltage, respectively).

The overall energy conversion efficiency η is defined as $\eta = (FF \times J_{sc} \times V_{oc})/P_{in}$, where P_{in} is the power of incident light.

Supporting Information (see also the footnote on the first page of this article): XRD, Raman spectroscopy, XPS, and SPS measurements, and UV/Vis spectra of N-doped TiO_2 powders.

Acknowledgments

This work was supported by the National Science Foundation of China (Grant No. 20671025 and 20771030), the China Postdoctoral Science Foundation Funded Project (No. 65204), and the Heilongjiang Provence Natural Science Foundation, China (No. B200603).

[1] B. O'Regan, M. Grätzel, *Nature* **1991**, *353*, 737.
[2] G. M. Lowman, P. T. Hammond, *Small* **2005**, *1*, 1070–1073.
[3] N. Ikeda, T. Miyasaka, *Chem. Commun.* **2005**, *5*, 1886–1888.
[4] Z. S. Wang, C. H. Huang, Y. Y. Huang, Y. J. Hou, P. H. Xie, B. W. Zhang, H. M. Cheng, *Chem. Mater.* **2001**, *13*, 678–682.
[5] J. M. Macak, M. Zlamal, J. Krysa, P. Schmuki, *Small* **2007**, *3*, 300–304.
[6] U. Bach, D. Lupo, P. Comte, *Nature* **1998**, *395*, 583–585.
[7] H. Q. Sun, Y. Bai, W. Q. Jin, N. P. Xu, *Sol. Energy Mater. Sol. Cells* **2008**, *92*, 76–83.
[8] E. Lancelle-Beltran, P. Prené, C. Boscher, P. Belleville, P. Buvat, S. Lambert, F. Guillet, C. Marcel, C. Sanchez, *Eur. J. Inorg. Chem.* **2008**, 903–910.
[9] M. R. Nunes, O. C. Monteiro, A. L. Castro, D. A. Vasconcelos, A. J. Silvestre, *Eur. J. Inorg. Chem.* **2008**, 961–965.
[10] S. Livraghi, M. C. Paganini, E. Giamello, A. Selloni, C. Di Valentin, G. Pacchioni, *J. Am. Chem. Soc.* **2006**, *128*, 15666–15671.
[11] S. H. Cheung, P. Nachimuthu, M. H. Engelhard, C. M. Wang, S. A. Chambers, *Surf. Sci.* **2008**, *602*, 133–141.
[12] S. A. Chambers, S. H. Cheung, V. Shutthanandan, S. Thevuthasan, M. K. Bowman, A. G. Joly, *Chem. Phys.* **2007**, *339*, 27–35.
[13] S. In, A. Orlov, R. Berg, F. Garcia, S. Pedrosa-Jimenez, M. S. Tikhov, D. S. Wright, R. M. Lambert, *J. Am. Chem. Soc.* **2007**, *129*, 13790–13791.
[14] R. Asahi, T. Morikawa, T. Ohwaki, K. Aoki, Y. Taga, *Science* **2001**, *293*, 269–271.
[15] R. Asahi, T. Morikawa, *Chem. Phys.* **2007**, *339*, 57–63.
[16] M. Batzill, E. H. Morales, U. Diebold, *Chem. Phys.* **2007**, *339*, 36–43.
[17] S. F. Chen, L. Chen, S. Gao, G. Y. Cao, *Chem. Phys. Lett.* **2005**, *413*, 404–409.
[18] X. M. Fang, Z. G. Zhang, Q. L. Chen, H. B. Ji, X. N. Gao, *J. Solid State Chem.* **2007**, *180*, 1325–1332.
[19] H. Chen, A. Nambu, W. Wen, J. Graciani, Z. Zhong, J. C. Hanson, E. Fujita, J. A. Rodriguez, *J. Phys. Chem. C* **2007**, *111*, 1366–1372.
[20] L. K. Randeniya, A. Bendavid, P. J. Martin, E. W. Preston, *J. Phys. Chem. C* **2007**, *111*, 18334–18340.
[21] K. Pomoni, A. Vomvas, C. Trapalis, *Thin Solid Films* **2008**, *516*, 1271–1278.
[22] J. G. Li, X. Yang, T. Ishigaki, *J. Phys. Chem. B* **2006**, *110*, 14611–14618.
[23] T. Ma, M. Akiyama, E. Abe, I. Imai, *Nano Lett.* **2005**, *5*, 2543–2547.
[24] N. G. Park, J. van de Lagemaat, A. J. Frank, *J. Phys. Chem. B* **2000**, *104*, 8989–8994.

[25] M. Miyauchi, A. Ikezawa, H. Tobimatsu, H. Irie, K. Hashimoto, *Phys. Chem. Chem. Phys.* **2004**, *6*, 865–870.
[26] H. Irie, Y. Watanabe, K. Hashimoto, *J. Phys. Chem. B* **2003**, *107*, 5483–5486.
[27] X. M. Qian, D. Q. Qin, Q. Song, Y. B. Bai, T. J. Li, X. Y. Tang, E. Wang, S. J. Dong, *Thin Solid Films* **2001**, *385*, 152–161.
[28] L. Q. Jing, X. J. Sun, J. Shang, W. M. Cai, Z. L. Xu, Y. G. Du, H. G. Fu, *Sol. Energy Mater. Sol. Cells* **2003**, *79*, 133–151.
[29] E. Barborini, A. M. Conti, I. Kholmanov, P. Piseri, A. Podestá, P. Milani, *Adv. Mater.* **2005**, *17*, 1842–1846.
[30] M. M. Oliveira, D. C. Schnitzler, A. J. G. Zarbin, *Chem. Mater.* **2003**, *15*, 1903–1909.
[31] T. Dittrich, I. Mora-Seró, G. García-Belmonte, J. Bisquert, *Phys. Rev. B* **2006**, *73*, 045407.

Received: February 8, 2009
Published Online: June 29, 2009

